

Fragmentation with a Cut on Thrust: Predictions for B-factories

Ambar Jain,^{a,b} Massimiliano Procura,^c Brian Shotwell,^d Wouter J. Waalewijn^d

^a*Department of Physics, Carnegie Mellon University, Pittsburgh, PA 15213, U.S.A.*

^b*Physics Department, Indian Institute of Science Education and Research, Bhopal, M.P. 462023, India*

^c*Albert Einstein Center for Fundamental Physics, Institute for Theoretical Physics, University of Bern, CH-3012 Bern, Switzerland*

^d*Department of Physics, University of California at San Diego, La Jolla, CA 92093, U.S.A.*

E-mail: ambarj@iiserb.ac.in, mprocura@itp.unibe.ch, bshotwell@ucsd.edu, wouterw@physics.ucsd.edu

ABSTRACT: The inclusion of B-factory data in fragmentation function analyses will improve the precision with which these are known. To remove the large b -quark contribution from on-resonance data, a cut on the thrust event shape T is used, leading to a dijet final state. Here we complete our analysis of unpolarized fragmentation of (light) quarks and gluons to a light hadron h with energy fraction z in $e^+e^- \rightarrow \text{dijet} + h$ at the center-of-mass energy $Q = 10.52$ GeV. In addition to the next-to-next-to-leading order resummation of logarithms of $1 - T$, we include the next-to-leading order (NLO) nonsingular $\mathcal{O}(1 - T)$ contribution to the cross section, the resummation of threshold logarithms of $1 - z$, and the leading nonperturbative contribution to the soft function. Our results can be directly used to study correlations between fragmentation and the thrust cut imposed on B-factory data, which must be taken into account to extract fragmentation functions with reliable uncertainties. These correlations are also observed in PYTHIA, but are surprisingly smaller at NLO.

Contents

1	Introduction	1
2	Calculating correlations between thrust and z in $e^+e^- \rightarrow \text{dijet} + h$	4
3	Numerical analysis for $e^+e^- \rightarrow \text{dijet} + \pi^+$	6
4	Studying τ^c-z correlations in Belle data	8
5	Conclusions	10
A	Nonsingular contribution at NLO	10
A.1	One-loop diagrams and kinematics	11
A.2	Quark and gluon fragmentation	11
A.3	Fragmentation with a thrust cut	12
A.4	NLO singular vs. nonsingular contribution	13
B	Choice of running scales	14
C	Perturbative coefficients C_j in moment space	15

1 Introduction

Hard QCD processes give rise to highly virtual partons that evolve by emitting radiation, until they hadronize into the nonperturbative states we observe. The physical basis of this “fragmentation” has not been constrained as much as jet production or deep-inelastic scattering (DIS), making this an active area of research. A quantitative understanding of parton fragmentation clearly extends the set of reactions that can be handled within a perturbative QCD approach. Applications include, for example, the investigation of the spin structure of the nucleon in semi-inclusive DIS [1, 2] and the study of hadron production at high p_T in pp collisions which is crucial to determine more accurately the relative suppression of hadron spectra (jet quenching) seen in heavy-ion collisions [3]. Interestingly, for many of these applications, additional cuts on the hadronic final state are required to reduce the background from other processes, to help identify underlying partonic structures or to have better control on the initial hard-scattering kinematics [1–6].

A key observation is that the fragmentation process involves physics at well-separated energy scales. It has been shown that high-energy processes with an observed hadron in the final state can be described by factorizing the short-distance (partonic) physics associated with

the hard scale Q , which is perturbatively calculable in QCD, from (universal) nonperturbative long-distance contributions, see *e.g.* ref. [7]. At leading power in Λ_{QCD}/Q , the (unpolarized) fragmentation functions (FFs) $D_i^h(z, \mu)$ [8, 9] encode the information on the nonperturbative transition from an energetic parton $i = \{g, u, \bar{u}, d, \dots\}$ to a hadron h , which carries a fraction z of its energy¹, plus a remainder X . The knowledge of both perturbative and nonperturbative ingredients in factorization theorems is crucial to obtain theoretical predictions. Unpolarized FFs, for example, serve as an input to extract the flavor separated helicity distributions from spin asymmetries observed in polarized semi-inclusive DIS [1–3].

Parameterizations for the FFs have been constrained by fitting to data for single-inclusive charged hadron production in e^+e^- at next-to-leading order (NLO) in perturbation theory [10–12]. More recently, global analyses have been performed to incorporate also semi-inclusive deep-inelastic scattering and/or pp , $p\bar{p}$ data from HERA, RHIC and the Tevatron [13–15]. To illustrate the current level of accuracy, the dominant $D_u^{\pi^+}(z, \mu = m_Z)$ is determined with uncertainties at the 10% level for $z \gtrsim 0.5$ [12]. The FFs of the gluon and the non-valence quarks are known even less accurately.

The Belle collaboration is currently studying light-quark fragmentation [16]. Since most of the current e^+e^- data is at $Q = m_Z$, this will significantly improve our knowledge of FFs. In particular, it will give access to the gluon FF via mixing with the quark FFs in the renormalization group evolution. To remove the large b -quark background in their high-statistics on-resonance data, the Belle collaboration imposes a cut on thrust, which is an event shape variable defined as [17]

$$T = \max_{\hat{t}} \frac{\sum_i |\hat{t} \cdot \vec{p}_i|}{\sum_i |\vec{p}_i|}, \quad (1.1)$$

where the sum is over all final-state particles. More precisely, it is found that a thrust cut of $\tau = 1 - T < 0.2$ removes 98% of the B data leaving the thrust distribution dominated by the fragmentation of light (u, d, s) and charmed quark pairs [18]. With this cut the hadronic final state is given by back-to-back jets.

In refs. [19–22] we developed the theoretical framework to study the fragmentation of a light parton into a light hadron h inside an identified jet. With “identified” we refer to jets determined either through an event shape like thrust [19, 20] or via a jet algorithm [22]. Our analysis provides the theoretical tools for a more exclusive study of fragmentation than is currently done, which is suitable for processes where additional cuts on the hadronic final states are imposed, such as the previous Belle example [18]. In particular, our framework allowed us to calculate the non-trivial correlations between τ^c and the energy fraction z in the observed cross section. Due to these correlations, the thrust cut modifies the shape in z . As already shown in the preliminary study of ref. [20], where we resummed the logarithms $\alpha_s^n \ln^m \tau$ to next-to-next-to-leading logarithmic accuracy (NNLL), the effect is expected to be sizable and important for the analysis of fragmentation in B-factory data. Here we improve

¹Due to perturbative radiation, the z in the fragmentation function is not the same as the experimentally measured momentum fraction [see *e.g.* eq. (2.1)].

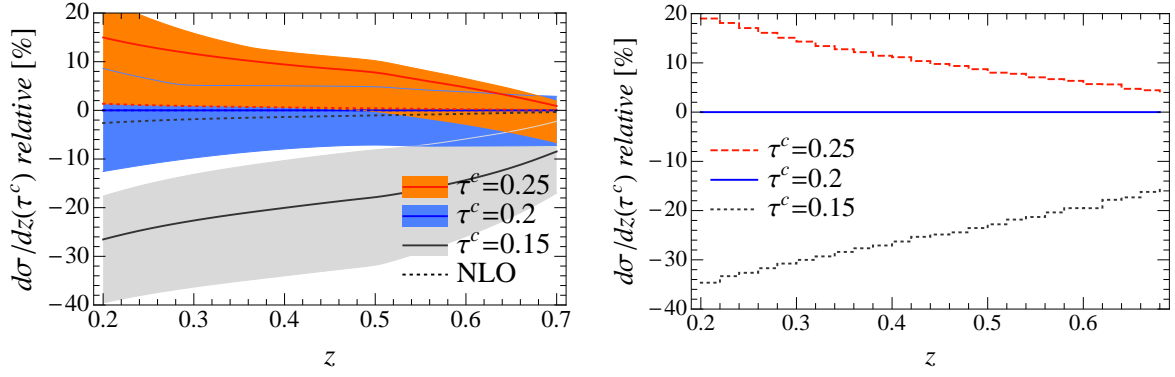


Figure 1. Correlations between the thrust cut $\tau \leq \tau^c$ and the observed momentum fraction z in the cross section of $e^+e^- \rightarrow \text{dijet} + \pi^+$ for $Q = 10.52$ GeV. Curves and bands are plotted relative to the case $\tau^c = 0.2$. A cut on thrust changes the shape in z . Left panel: our NNLL+NLO results with perturbative uncertainty bands. The result at NLO (dotted lines) contains negligible correlations. As input we use the HKNS fragmentation functions $D_i^{\pi^+}$ [12] at NLO. Right panel: the same observable using PYTHIA.

our study in ref. [20] by including the NLO nonsingular contribution to the cross section, the resummation of threshold logarithms of $1 - z$ and the leading nonperturbative correction to the thrust soft function, which are discussed in sec. 2.

The correlations we obtain from our new analysis are shown in the left panel of fig. 1 for various thrust cuts τ^c , including the theoretical (perturbative) uncertainties. As can be seen there, the effect of the thrust cut τ^c is much stronger in the small z region than in the large z region. This has a straightforward physical explanation: for larger values of z , most of the jet energy is carried by the observed hadron, causing the jet to be more collimated and less affected by the thrust cut. In particular, for $z \geq 1 - \tau^c$, the cross section is unaffected by the thrust cut. On comparison with the right panel, we see that the effect we find is fully compatible with the outcome of the PYTHIA event generator based on LL parton showering and the Lund string fragmentation model². We stress that the plot in the left panel has been obtained from our purely perturbative calculation, taking only the phenomenological parameterization of the universal $D_i^{\pi^+}$ in ref. [12] as input. There we also show the correlations that we obtain at NLO (dotted curves), which are much smaller. Presumably, the single additional emission at NLO is insufficient to reliably describe this doubly-differential cross section, compared to the multiple emissions in our resummed calculation and in PYTHIA. The purpose of our study is to pave the way for a reliable extraction of the light-quark fragmentation functions using high-statistics on-resonance B-factory data, with controllable theoretical uncertainties.

The paper is organized as follows. In sec. 2 we briefly review our theoretical framework, where we describe the updates of our analysis compared to our previous work in ref. [20]. In

²The results for other light hadrons, like the proton, are very similar to the ones shown here for π^+ .

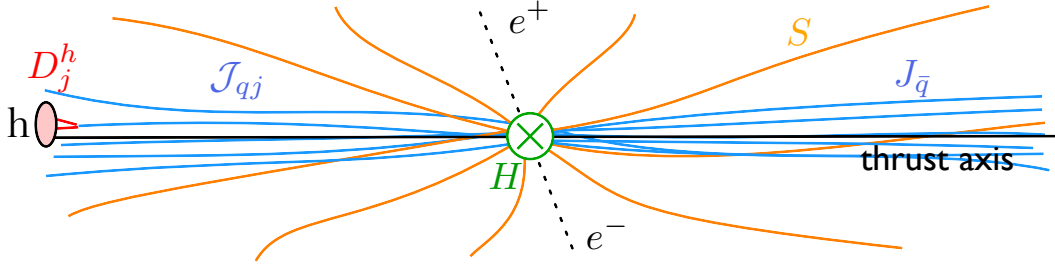


Figure 2. A schematic of the various subprocesses in $e^+e^- \rightarrow \text{dijet} + h$: The (green) vertex denotes the hard interaction H , the (blue) jets are described by J and \mathcal{J}_{ij} (the latter for the jet in which the hadron is observed), the fragmentation $j \rightarrow h$ is described by the fragmentation function D_j^h and the effects of the (orange) soft radiation are contained in S .

sec. 3 we discuss the features of the z -spectrum and τ -spectrum and illustrate the effect of the different ingredients of our calculation. In sec. 4 we propose a first, straightforward, quantitative analysis of correlations between z and τ^c in Belle data. All the necessary theoretical input for this moment-space analysis is collected in app. C. App. A contains the details of the calculation of the NLO nonsingular contribution to the cross section. A detailed discussion of our choice of renormalization scales, as well as the scale variations used to estimate the perturbative uncertainties, is given in app. B.

2 Calculating correlations between thrust and z in $e^+e^- \rightarrow \text{dijet} + h$

We focus on the case of spin-averaged fragmentation in $e^+e^- \rightarrow \text{dijet} + h$ where one restricts to the dijet limit by a cut on thrust. Starting from the well-known factorization theorem for the inclusive measurement of thrust [23–26], in refs. [19, 20] we obtained a factorization theorem for the observed cross section at leading power in Λ_{QCD}/Q , which has this form:

$$\frac{d\sigma^h}{dz}(\tau^c) = \int_0^{\tau^c} d\tau \frac{d^2\sigma^h}{d\tau dz} = \sum_{j=g,u,\bar{u},d,\dots} \int_z^1 \frac{dx}{x} D_j^h(x, \mu) C_j\left(\tau^c, \frac{z}{x}, Q^2, \mu\right). \quad (2.1)$$

Q is the center-of-mass energy. The $D_j^h(x)$ denote the standard, unpolarized fragmentation functions, which describe the hadronization $j \rightarrow h(x)$ at leading power. The index j runs over all parton flavors, including the gluon. The coefficients C_j are calculable in perturbation theory and contain double logarithms of τ^c , $\alpha_s^n \ln^m \tau^c$ ($m \leq 2n$), and “threshold” logarithms of $1 - z$. Our setup enables us to resum all these large logarithms in the dijet region of the thrust distribution, which is relevant for B-factories. This is necessary to achieve perturbative convergence with small uncertainties in C_j when $\tau^c \lesssim 0.2$ and when $z \gtrsim 0.5$, as we will show in sec. 3. The scale μ in eq. (2.1) is arbitrary, but must be chosen to be the same in C_j and D_j^h .

We obtained the expression for C_j by exploiting factorization in the framework of soft-collinear effective theory [27–30]. The underlying idea is that dynamics at well-separated

scales combine incoherently, allowing one to factorize their contributions to the cross section. In the dijet region, the relevant scales and the subprocesses they correspond to are illustrated in fig. 2 and eq. (2.2). Specifically, we distinguish the scale Q for the hard collision $e^+e^- \rightarrow q\bar{q}$, the scale $\sqrt{\tau^c}Q$ for the jet production (showering), the scale $\tau^c Q$ associated with the soft radiation between the jets, and the scale Λ_{QCD} at which hadronization takes place. The coefficients $C_j(\tau^c, Q^2, x/z, \mu)$ are given by the convolution of functions encoding the effects at these different perturbative scales plus a nonsingular piece which contains contributions that do not factor in this way. Schematically,

$$C_j\left(\tau^c, Q^2, \frac{x}{z}, \mu\right) = \sum_q \sigma_0^q H(Q^2) \left[\mathcal{J}_{qj}(\tau^c Q^2, x/z) \otimes J_{\bar{q}}(\tau^c Q^2) + J_q(\tau^c Q^2) \otimes \mathcal{J}_{\bar{q}j}(\tau^c Q^2, x/z) \right] \\ \otimes S_\tau\left((\tau^c)^2 Q^2\right) \left\{ 1 + \mathcal{O}\left[\frac{\Lambda_{\text{QCD}}^2}{(1-z)\tau^c Q^2}, \left(\frac{\Lambda_{\text{QCD}}}{\tau^c Q}\right)^2\right] \right\} + C_j^{\text{ns}}\left(\tau^c, Q^2, \frac{x}{z}, \mu\right), \quad (2.2)$$

where σ_0^q is the tree-level cross section. Since it is not known whether the observed hadron h fragmented from the quark or the antiquark jet, we sum over both possibilities. The C_j^{ns} contains the terms of the NLO cross section that are not enhanced by logarithms of τ , and is $\mathcal{O}(\tau)$ suppressed. The calculation of the nonsingular contribution to $d^2\sigma^h/(d\tau dz)$ at NLO is discussed in detail in app. A and its numerical effects are shown in sec. 3. All the other ingredients in the C_j 's have been calculated in the literature to some order in the perturbative expansion. We refer to [20] for details. In particular, our one-loop determination of the coefficients \mathcal{J}_{ij} in ref. [20] (partly contained also in ref. [31]) enabled us to analyze the cross section in eq. (2.1) up to NNLL accuracy. We stress that since fragmentation takes place inside a (hemisphere) jet of invariant mass of order $\tau^c Q^2$, the momentum fraction z cannot be too small, to avoid contributions from soft hadrons outside the jet. The hadron momentum must be larger than the soft scale, implying $z \gtrsim \tau^c$.

The factorization in eq. (2.2) enables the resummation of logarithms of τ and $1-z$, as well as large π^2 terms in H , which is accomplished by evaluating H , \mathcal{J}_{ij} , J and S at their natural scales and using their respective RGEs to evolve them to a common scale μ . We have made improvements in our choice of scales compared to our earlier work in ref. [20], specifically, we resum threshold logarithms and take the upperbound $\tau \leq 1-z$ into account. A detailed discussion of our choice running scales is deferred to app. B.

We now comment on the various corrections in eq. (2.2). There are corrections of order $\Lambda_{\text{QCD}}^2/[(1-z)\tau^c Q^2]$ associated with the \mathcal{J}_{ij} 's. These coefficients describe the emissions from the parent parton (here a quark) at large virtualities building up the jet in which the hadron is identified. The associated corrections get sizable if the jet invariant mass gets small. In our plots in sec. 3 we have included the leading nonperturbative contribution to S_τ , according to the analysis in ref. [32], which pushes the nonperturbative corrections to the soft function to order $\Lambda_{\text{QCD}}^2/(\tau^c Q)^2$, as indicated in eq. (2.2). These nonperturbative corrections become large for small τ^c , up to about 15% for $\tau^c = 0.15$. We therefore need τ^c to be not too small.

Quark and hadron masses are treated as negligible in our calculation, and we briefly comment on the size of the corresponding kinematic corrections. The corrections due to the hadron mass m_h are of order $m_h^2/(z^2 Q^2)$ [33]. For light hadrons, like pions and kaons, they are indeed negligible in the region where our framework can be applied. In the plots of sec. 3, we restrict q in eq. (2.2) to be u, d, s . The correction due to the charm mass is expected to be of order $m_c^2/(\tau^c Q^2)$ when charm is a valence quark, which is less significant than the other corrections to eq. (2.2). If the hadron h does not contain a charm valence quark, the only contribution to eq. (2.1) that does not get further suppressed by the smallness of the corresponding FF, is the one involving D_g^h .

3 Numerical analysis for $e^+e^- \rightarrow \text{dijet} + \pi^+$

Here we illustrate our key results for the cross-section in $e^+e^- \rightarrow \text{dijet} + \pi^+$, given in eq. (2.1). As input we use the HKNS fragmentation functions $D_q^{\pi^+}$ and $D_g^{\pi^+}$ [12] at NLO. To be consistent with ref. [12], we set $\alpha_s(\mu = m_Z) = 0.125$ with two-loop running, matching continuously across the quark thresholds³. In our analysis we do not include the effects of the uncertainties associated with $\alpha_s(m_Z)$ or with the FF parameters. Therefore we stress that the bands shown in our plots correspond only to the perturbative uncertainties obtained from scale variations, as explained in app. B.

We have made the following improvements with respect to the plots shown in ref. [20]:

- (a) We include the NLO nonsingular contribution, which we calculate in app. A. This small $\mathcal{O}(\tau)$ correction plays a role for $\tau^c \gtrsim 0.2$.
- (b) We resum the threshold logarithms of $1 - z$ according to our ref. [22], where we introduced a joint resummation of these logarithms and those in τ^c (suitable for values of τ^c in the range of interest for Belle). As described in app. B, this is accomplished through the choice of the renormalization scale for \mathcal{J}_{ij} . These effects are important for $z \gtrsim 0.5$.
- (c) We include the leading nonperturbative correction to S_τ according to ref. [32]. This amounts to a shift in the thrust distribution, $\tau^c \rightarrow \tau^c - 2\bar{\Omega}_1/Q$, where $\bar{\Omega}_1 = 0.252 \text{ GeV}$ in the $\overline{\text{MS}}$ scheme. The effect of this is most prominent at small τ^c .

In figs. 3 and 4 the effects of the thrust cut and our resummations are illustrated for fixed values of z . As the cut becomes stronger (i.e. for smaller τ^c) the cross section gets reduced, and by a larger amount in the case of our resummed calculation. For $\tau^c \lesssim 0.2$ our resummed result starts to differ from the leading order (LO) and NLO results, showing the effect of the resummation of double logarithms of τ^c and the leading nonperturbative correction.

The nonsingular NLO correction is singled out in fig. 4, where we switch off both the threshold resummation and the resummation of π^2 -terms in the hard factor H of eq. (2.2). The nonsingular contribution is not large, but it causes our resummed calculation to merge

³In the next sections, which do not involve HKNS FFs, we will use a more realistic value for α_s .

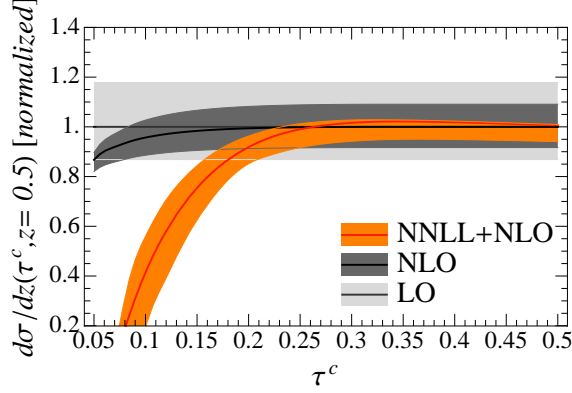


Figure 3. The effect of the thrust cut in $e^+e^- \rightarrow \text{dijet} + \pi^+$ for $Q = 10.52$ GeV and $z = 0.5$ at LO, NLO and NNLL+NLO. The curves are normalized at $\tau^c = 0.5$. The bands show the perturbative uncertainties obtained from scale variations discussed in app. B.

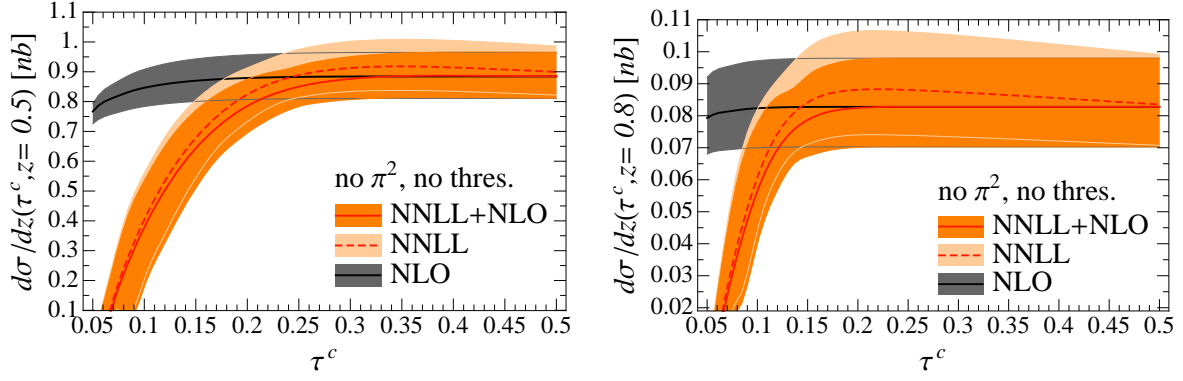


Figure 4. The effect of the inclusion of the NLO nonsingular contribution is illustrated for $z = 0.5$ (left panel) and $z = 0.8$ (right panel), with π^2 and threshold resummations switched off.

with the NLO in the $\tau^c \rightarrow 0.5$ region where resummation is unimportant, and removes an unphysical decrease of the integrated cross-section for large values of τ^c . If we include threshold and π^2 resummation, we should also include these resummation in the nonsingular contribution to the cross section, to preserve the above properties. Following ref. [34], we estimate the π^2 resummation of the nonsingular (which is formally higher order in α_s) by simply multiplying it with the corresponding evolution of the hard function $U_H(Q^2, \mu_H, |\mu_H|)$, given in eq. (C.7) of ref. [20]. We have not attempted to resum the threshold logarithms in the nonsingular, so our calculation does not (yet) reliably describe the region where *both* τ and z are large.

Next, we look at the effect of the thrust cut on the z spectrum (“the shape of the fragmentation function”), which is shown in figs. 5 and 6 for the default value $\tau^c = 0.2$. In fig. 5 we compare our resummed result at next-to-leading logarithmic order (NLL) and NNLL+NLO with and without threshold resummation. The threshold resummation leads

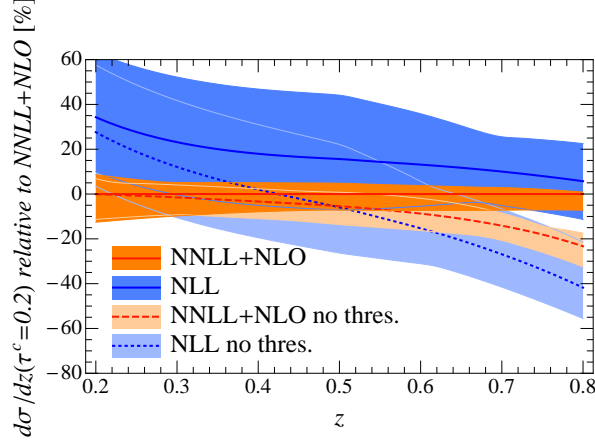


Figure 5. Comparison of NLL and NNLL+NLO with/without threshold resummation, for $\tau^c = 0.2$.

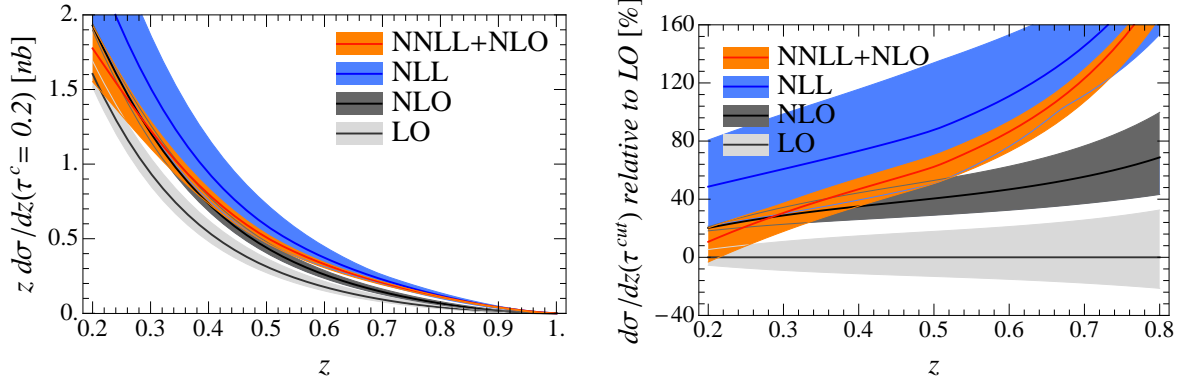


Figure 6. The effect of the thrust cut $\tau^c = 0.2$ on the z -spectrum for $e^+e^- \rightarrow \text{dijet} + \pi^+$ with $Q = 10.52$ GeV at LO, NLO, NLL and NNLL. The right panel shows the curves and bands in the left panel relative to the central curve for the LO result.

to slightly better convergence and smaller uncertainties at NNLL+NLO for $z \gtrsim 0.5$. The effect is not as dramatic as in ref. [22] because the scales are much smaller here. In fig. 6 we compare our NLO, NLL and NNLL+NLO curves with the LO result, which is independent of τ^c . The differences between the shape in z are not entirely due to the thrust cut, but also correspond to different orders in (resummed) perturbation theory. As is clear from fig. 1, we also find correlations between τ^c and z . These effects have to be taken into account when a fit to experimental data is performed to *extract* the FFs.

4 Studying τ^c - z correlations in Belle data

In fig. 1 and sec. 3 we showed that the thrust cut has a sizable, calculable effect on the spectrum of the fragmentation variable z . Our framework allows one to study this qualitatively *and* quantitatively in the Belle data.

For a first quantitative analysis, we propose working in moment space, where eq. (2.1) simplifies to

$$\int_0^1 dz z^{N-1} \frac{d\sigma^h}{dz}(\tau^c) = \sum_j \tilde{D}_j^h(N, \mu) \tilde{C}_j(\tau^c, N, Q, \mu), \quad (4.1)$$

with

$$\tilde{D}_j^h(N, \mu) = \int_0^1 dx x^{N-1} D_j^h(x, \mu). \quad (4.2)$$

At variance with eq. (2.1), we use the notation $j = q, g$ by defining

$$\tilde{D}_q^h = Q_u^2(D_u^h + D_{\bar{u}}^h + D_c^h + D_{\bar{c}}^h) + Q_d^2(D_d^h + D_{\bar{d}}^h + D_s^h + D_{\bar{s}}^h), \quad \tilde{C}_q = \tilde{C}_u/Q_u^2 \approx \tilde{C}_d/Q_d^2, \quad (4.3)$$

with $Q_u = 2/3$ and $Q_d = -1/3$ the electric charges of the up- and down-type quarks. In app. C we collect our numerical values for $\tilde{C}_j(\tau^c, N, Q = 10.52 \text{ GeV}, \mu = 1 \text{ GeV})$ in nanobarns for $j = q, g$, $\tau^c = 0.15, 0.16, \dots, 0.2$ and $N = 3, 4, \dots, 8$, at NNLL+NLO. We use $\alpha_s(m_Z) = 0.118$ and three-loop running⁴, and employ two-loop splitting functions [35–37] to evolve to $\mu = 1 \text{ GeV}$. We provide a different set of coefficients for each of the independent scale variations in app. B, which allows one to take correlations between the uncertainties into account.

Apart from the different electric charges for the up- and down-type quarks, the difference between \tilde{C}_u and \tilde{C}_d is less than one percent. Thus the thrust cut does not provide a way to extract FFs for different quark flavors, but gives access only to the combination in eq. (4.3). Varying the thrust cut allows one in principle to separate out the gluon contribution. However, at the scale $\mu = 1 \text{ GeV}$, where the fragmentation functions are usually extracted, this contribution to the cross section is small and dominated by uncertainties.

Taking as input the Belle spectra, where both τ^c and z are varied, the numbers in tables 2 and 3 can be directly used to perform fits for the moments $\tilde{D}_q(N, \mu = 1 \text{ GeV})$. If these fits produce acceptable values of $\chi^2/\text{d.o.f.}$, the next step will be the more involved analysis of correcting the measured z -spectra for the effect of the thrust cut, to reliably extract the FFs. Note that Mellin moment methods have been used in analyzing fragmentation functions before [13, 14]. We stress that our formalism enables one to use data at different τ^c to better constrain the parameters for the FFs.

Experimentally, using moments has the disadvantage that they can be sensitive to the problematic $z \lesssim 0.2$ region, and the $z \gtrsim 0.9$ region, where the experimental uncertainties are large [16]. The relative contribution of these regions to the moments of $D_u^{\pi^+}$ and $D_d^{\pi^+}$ is shown in fig. 7. This is why we restricted ourselves here to moments in the range $3 \leq N \leq 8$. In addition, the thrust cut should neither be too soft (contamination with b quarks) nor too strong (reduced signal). As we explained in sec. 2, the requirements for our calculation to be under theoretical control are similar.

⁴To avoid crossing flavor thresholds in our calculation, we choose to move the charm and bottom thresholds outside the range of scales that we work in.

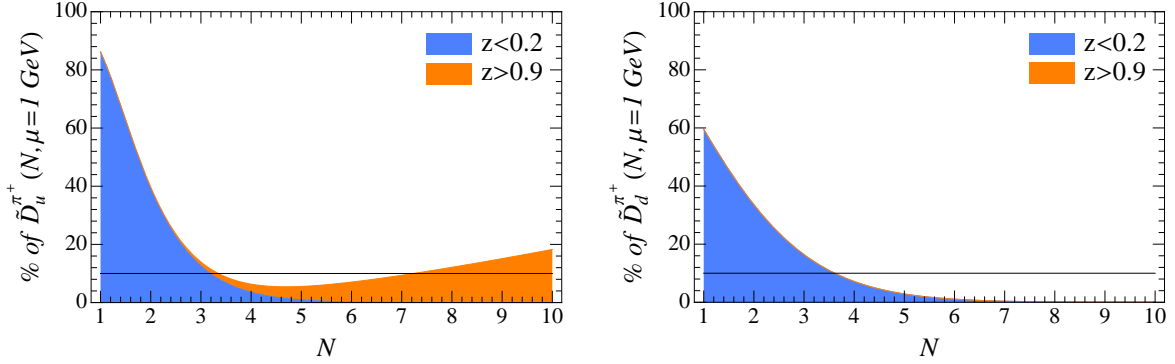


Figure 7. The composition of the N th moment of $D_u^{\pi^+}$ (left panel) and $D_d^{\pi^+}$ (right panel). Using different colors we show the contribution from the problematic regions $z < 0.2$ and $z > 0.9$. The contribution from $z > 0.9$ for d quarks is very small and hardly visible.

5 Conclusions

We have studied the cross section for fragmentation with a thrust cut, which is relevant to analyze fragmentation in high-statistics on-resonance B-factory data. The shape of the cross section in z is altered beyond LO and includes a τ -dependent contribution. The correlation between τ and z found in our resummed calculation is observed in PYTHIA as well, but is much smaller at NLO. Our plots in secs. 1 and 3 and the discussion in sec. 4 provide the starting point for a qualitative and quantitative analysis of this effect. We emphasize that binning the data in τ^c allows one to study the correlations in τ^c and z , and leads to more stringent fits for the fragmentation functions.

Acknowledgments

We thank M. Grosse Perdekamp for helpful discussions. M.P. acknowledges support by the “Innovations- und Kooperationsprojekt C-13” of the Schweizerische Universitätskonferenz SUK/CRUS and by the Swiss National Science Foundation. W.W. is supported by DOE grant DE-FG02-90ER40546.

A Nonsingular contribution at NLO

We obtain the NLO nonsingular correction to the cross section for $e^+e^- \rightarrow \text{dijet} + h$, by subtracting the singular $\ln^m \tau^c$ terms from the full NLO calculation. The singular NLO can directly be obtained from our resummed calculation in ref. [20], so we start by calculating the full NLO cross section. Although most ingredients are well-known, we include them here for completeness.

A.1 One-loop diagrams and kinematics

We perform the calculation using dimensional regularization for the UV and IR divergences in the $\overline{\text{MS}}$ scheme. The tree-level cross section $e^+e^- \rightarrow q\bar{q}$ is given by

$$\sigma^{(0)} = \frac{4\pi\alpha^2 N_c}{3q^2} + \mathcal{O}(\epsilon). \quad (\text{A.1})$$

The real and virtual contribution at one loop are [38]

$$\begin{aligned} \sigma_R^{(1)} &= \sigma^{(0)} \frac{\alpha_s C_F}{\pi} \frac{e^{\epsilon\gamma_E}}{2\Gamma(1-\epsilon)} \left(\frac{\mu^2}{q^2}\right)^\epsilon \int \prod_i [dx_i (1-x_i)^{-\epsilon}] \delta(2-x_1-x_2-x_3) \frac{x_1^2+x_2^2-\epsilon x_3^2}{(1-x_1)(1-x_2)}, \\ \sigma_V^{(1)} &= \sigma^{(0)} \frac{\alpha_s C_F}{\pi} \left(\frac{\mu^2}{q^2}\right)^\epsilon \left[-\frac{1}{\epsilon^2} - \frac{3}{2\epsilon} - 4 + \frac{7\pi^2}{12} \right]. \end{aligned} \quad (\text{A.2})$$

We employ the usual parametrization for the $e^+e^- \rightarrow q\bar{q}g$ final state

$$x_i = \frac{2p_i \cdot q}{q^2} \stackrel{\text{CMS}}{=} \frac{2p_i^0}{q^0}, \quad 0 \leq x_i \leq 1, \quad x_1 + x_2 + x_3 = 2, \quad (\text{A.3})$$

where q is the momentum of the e^+e^- pair and the $p_{i=1,2,3}$ are the momenta of the quark, anti-quark and gluon, respectively. The phase-space integration boundaries for the real emission $\sigma_R^{(1)}$ in eq. (A.2) depend on the observable. These are quite simple for the observables we are interested in: the x_i are the momentum fractions and thrust $T = 1 - \tau = \max\{x_1, x_2, x_3\}$.

A.2 Quark and gluon fragmentation

We first consider the cross section where only the momentum fraction z of the hadron h is observed. This is described by the factorization theorem

$$\frac{d\sigma_h}{dz} = \sum_{i=q,\bar{q},g} \int_z^1 \frac{dx}{x} \frac{d\hat{\sigma}_i}{dx} D_i^h\left(\frac{z}{x}\right), \quad (\text{A.4})$$

up to Λ_{QCD}/Q power corrections. Replacing h by a quark or a gluon, we find at one-loop order that

$$\begin{aligned} \frac{d\sigma_q^{(1)}}{dz} &= \int \frac{dx}{x} \left[\frac{d\hat{\sigma}_q^{(0)}}{dx} D_q^{q(1)}\left(\frac{z}{x}\right) + \frac{d\hat{\sigma}_q^{(1)}}{dx} D_q^{q(0)}\left(\frac{z}{x}\right) \right] \\ &= -\sigma^{(0)} \frac{1}{\epsilon_{\text{IR}}} \frac{\alpha_s C_F}{2\pi} P_{qq}(z) + \frac{d\hat{\sigma}_q^{(1)}}{dz}, \\ \frac{d\sigma_g^{(1)}}{dz} &= \int \frac{dx}{x} \left[\frac{d\hat{\sigma}_q^{(0)}}{dx} D_q^{g(1)}\left(\frac{z}{x}\right) + \frac{d\hat{\sigma}_{\bar{q}}^{(0)}}{dx} D_{\bar{q}}^{g(1)}\left(\frac{z}{x}\right) + \frac{d\hat{\sigma}_g^{(0)}}{dx} D_g^{g(0)}\left(\frac{z}{x}\right) \right] \\ &= -\sigma^{(0)} \frac{1}{\epsilon_{\text{IR}}} \frac{\alpha_s C_F}{\pi} P_{gq}(z) + \frac{d\hat{\sigma}_g^{(1)}}{dz}, \end{aligned} \quad (\text{A.5})$$

restricting to one quark flavor for simplicity. Here we used that

$$\frac{d\hat{\sigma}_q^{(0)}}{dx} = \sigma^{(0)}\delta(1-x), \quad \frac{d\hat{\sigma}_g^{(0)}}{dx} = 0, \quad (\text{A.6})$$

as well as the partonic fragmentation functions in pure dimensional regularization,

$$\begin{aligned} D_q^q(z) &= \delta(1-z) + \frac{\alpha_s C_F}{2\pi} P_{qq}(z) \left(\frac{1}{\epsilon_{\text{UV}}} - \frac{1}{\epsilon_{\text{IR}}} \right), & D_q^g(z) &= \frac{\alpha_s C_F}{2\pi} P_{gq}(z) \left(\frac{1}{\epsilon_{\text{UV}}} - \frac{1}{\epsilon_{\text{IR}}} \right), \\ D_g^g(z) &= \delta(1-z) + \mathcal{O}(\alpha_s). \end{aligned} \quad (\text{A.7})$$

The one-loop splitting functions are [39]

$$P_{qq}(z) = \left(\frac{1+z^2}{1-z} \right)_+ = \frac{1+z^2}{(1-z)_+} + \frac{3}{2}\delta(1-z), \quad P_{gq}(z) = \theta(1-z) \frac{1+(1-z)^2}{z}. \quad (\text{A.8})$$

Measuring the momentum fraction of the (anti)quark or gluon, the real radiation contribution in eq. (A.2) becomes

$$\begin{aligned} \frac{d\sigma_{q,R}^{(1)}}{dz} &= \sigma^{(0)} \frac{\alpha_s C_F}{\pi} \left(\frac{\mu^2}{q^2} \right)^\epsilon \left\{ \frac{1}{\epsilon^2} \delta(1-z) + \frac{1}{\epsilon} \left[\frac{3}{2} \delta(1-z) - \frac{1}{2} P_{qq}(z) \right] + \right. \\ &\quad \left. (1+z^2) \left[\frac{1}{2} \left(\frac{\ln(1-z)}{1-z} \right)_+ + \frac{\ln z}{1-z} \right] - \frac{3}{4} \frac{1}{(1-z)_+} + \delta(1-z) \left(\frac{7}{4} - \frac{\pi^2}{4} \right) - \frac{3}{4} z + \frac{5}{4} \right\}, \\ \frac{d\sigma_{g,R}^{(1)}}{dz} &= \sigma^{(0)} \frac{\alpha_s C_F}{\pi} \left(\frac{\mu^2}{q^2} \right)^\epsilon P_{gq}(z) \left[-\frac{1}{\epsilon} + \ln(1-z) + 2 \ln z \right]. \end{aligned} \quad (\text{A.9})$$

The virtual piece in eq. (A.2) gives a contribution $\sigma_V^{(1)}\delta(1-z)$ to $\sigma_q^{(1)}$, which largely cancels the divergences of $\sigma_{q,R}^{(1)}$. The remaining infrared divergences are exactly those required by eq. (A.5), and the finite terms yield

$$\begin{aligned} \frac{d\hat{\sigma}_{q,R}^{(1)}}{dz} &= \sigma^{(0)} \frac{\alpha_s C_F}{\pi} \left\{ -\frac{1}{2} P_{qq}(z) \ln \frac{\mu^2}{q^2} + (1+z^2) \left[\frac{1}{2} \left(\frac{\ln(1-z)}{1-z} \right)_+ + \frac{\ln z}{1-z} \right] - \frac{3}{4} \frac{1}{(1-z)_+} + \right. \\ &\quad \left. \delta(1-z) \left(\frac{\pi^2}{3} - \frac{9}{4} \right) - \frac{3}{4} z + \frac{5}{4} \right\}, \\ \frac{d\hat{\sigma}_g^{(1)}}{dz} &= \sigma^{(0)} \frac{\alpha_s C_F}{\pi} P_{gq}(z) \left[-\ln \frac{\mu^2}{q^2} + \ln(1-z) + 2 \ln z \right]. \end{aligned} \quad (\text{A.10})$$

This agrees with the calculations performed a long time ago in refs. [36, 37, 40].

A.3 Fragmentation with a thrust cut

The easiest way to calculate the fragmentation cross section with a thrust cut at NLO is

$$\frac{d\sigma_h}{dz}(\tau \leq \tau^c) = \frac{d\sigma_h}{dz} - \frac{d\sigma_h}{dz}(\tau \geq \tau^c). \quad (\text{A.11})$$

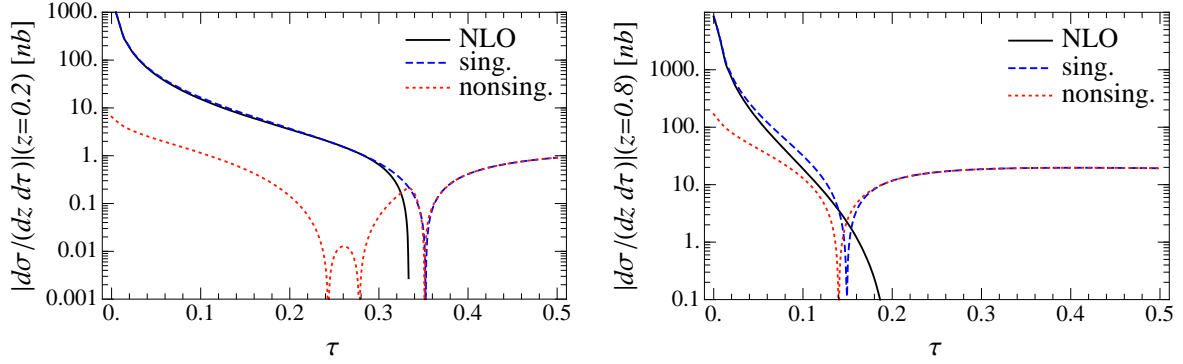


Figure 8. The cross section for $e^+e^- \rightarrow \text{dijet} + \pi^+$ at $Q = 10.52$ GeV, differential in the momentum fraction z and thrust τ , and separated into its singular and nonsingular contribution. Since these separate pieces can be negative, absolute values are plotted.

The first term on the right-hand side was calculated in the previous section. The second term is described by a factorization theorem very similar to eq. (A.4)

$$\frac{d\sigma_h}{dz}(\tau \geq \tau^c) = \sum_{i=q,\bar{q},g} \int_z^1 \frac{dx}{x} \frac{d\hat{\sigma}_i}{dx}(\tau \geq \tau^c) D_i^h\left(\frac{z}{x}\right). \quad (\text{A.12})$$

At NLO the thrust cut removes any regions of phase-space involving divergences, so we may set $\epsilon = 0$. Only the real radiation contributes, yielding

$$\begin{aligned} \frac{d\hat{\sigma}_q}{dz}(\tau \geq \tau^c) &= \sigma^{(0)} \frac{\alpha_s C_F}{2\pi} \theta(1-z-\tau^c) \theta(z-2\tau^c) \int_{1-z+\tau^c}^{1-\tau^c} dx \frac{z^2+x^2}{(1-z)(1-x)} \\ &= \sigma^{(0)} \frac{\alpha_s C_F}{\pi} \theta(1-z-\tau^c) \theta(z-2\tau^c) \left[\frac{1}{2} P_{qq}(z) \ln \frac{z-\tau^c}{\tau^c} + \frac{z^2-2z(\tau^c+2)+8\tau^c}{4(1-z)} \right], \\ \frac{d\hat{\sigma}_g}{dz}(\tau \geq \tau^c) &= \sigma^{(0)} \frac{\alpha_s C_F}{2\pi} \theta(1-z-\tau^c) \theta(z-2\tau^c) \int_{1-z+\tau^c}^{1-\tau^c} dx \frac{(2-x-z)^2+x^2}{(x+z-1)(1-x)} \\ &= \sigma^{(0)} \frac{\alpha_s C_F}{\pi} \theta(1-z-\tau^c) \theta(z-2\tau^c) \left[P_{gq}(z) \ln \frac{z-\tau^c}{\tau^c} - z + 2\tau^c \right]. \end{aligned} \quad (\text{A.13})$$

A.4 NLO singular vs. nonsingular contribution

The singular cross section can directly be obtained from our resummed calculation in eq. (2.2), by choosing the renormalization scale of all the objects equal to μ , which switches off the resummation. By subtracting this from the NLO cross section calculated in the previous section, we obtain the nonsingular piece. In fig. 8 the NLO cross section for $z = 0.2$ and $z = 0.8$ is shown separated into its singular and nonsingular contribution. A first cross-check of our calculation is provided by the fact that the nonsingular piece is finite in the $\tau \rightarrow 0$ limit, whereas both the full NLO and the singular piece diverge. The contribution of the nonsingular to the total cross section is suppressed for small τ by $\mathcal{O}(\tau)$. However, for larger

values of τ its contribution becomes more important, and above the NLO kinematic threshold $\tau \geq \min\{1/3, 1 - z\}$ the total cross section vanishes and the singular and nonsingular exactly cancel each other. It is in this region that the inclusion of the nonsingular is essential to avoid a negative differential cross section in τ or an unphysical turn-over in the cross section integrated up to $\tau \leq \tau^c$.

B Choice of running scales

The resummation of logarithms of τ and $1 - z$, as well as large π^2 terms, is accomplished by evaluating H , J , \mathcal{J} and S in eq. (2.2) at their natural scales μ_H , μ_J , $\mu_{\mathcal{J}}$, μ_S , and using their respective RGEs to evolve them to a common scale μ . Having made some improvements compared to our earlier work ref. [20], we discuss this in some detail here.

The hard function H is the square of a time-like form factor and contains large π^2 -terms at $\mu_H = Q$ arising from $\ln^2(-iQ/\mu_H)$. These can be resummed through the complex scale setting $\mu_H = -iQ$ [41–44]. Following ref. [32], we note that there are three distinct kinematic regions where the resummation of the logarithms of τ must be handled differently:

- 1) $\mu_H \simeq -iQ$, $\mu_J \simeq \sqrt{\Lambda_{\text{QCD}}Q}$, $\mu_S = \Lambda_{\text{QCD}}$,
- 2) $\mu_H \simeq -iQ$, $\mu_J \simeq \sqrt{\tau}Q$, $\mu_S \simeq \tau Q$,
- 3) $i\mu_H = \mu_J = \mu_S \simeq Q$.

Region 1) is not of interest for our application, and requires a completely nonperturbative soft function. The resummation of the threshold logarithms of $1 - z$ sets the scale $\mu_{\mathcal{J}}$ different from μ_J for the *diagonal* terms \mathcal{J}_{qq} [22]. In addition, the measurement of z affects the upper bound $\tau \leq \tau_{\text{max}} = \min\{0.5, 1 - z\}$, implying that region 3) sets in at smaller values of τ for $z > 0.5$. Taking this into account, a smooth transition between the three regions is given by

$$\begin{aligned}
\mu_H &= -ie_H Q, \\
\mu_J(\tau, z) &= \left[1 + e_J \theta(r_3 \tau_{\text{max}} - \tau) \left(1 - \frac{\tau}{r_3 \tau_{\text{max}}} \right)^2 \right] \sqrt{|\mu_H| \mu_{\text{run}}(\tau/\tau_{\text{max}}, z, |\mu_H|)}, \\
\mu_{\mathcal{J}}(\tau, z) &= \sqrt{1 - z} \mu_J(\tau, z), \\
\mu_S(\tau, z) &= \left[1 + e_S \theta(r_3 \tau_{\text{max}} - \tau) \left(1 - \frac{\tau}{r_3 \tau_{\text{max}}} \right)^2 \right] \mu_{\text{run}}(\tau/\tau_{\text{max}}, z, |\mu_H|), \tag{B.1}
\end{aligned}$$

where scale uncertainties will be estimated by varying e_H , e_J and e_S as shown in table 1. In addition to the explicit z -dependence in $\mu_{\mathcal{J}}$, there is an implicit dependence through τ_{max} . For the profile $\mu_{\text{run}}(\tau/\tau_{\text{max}}, z, |\mu_H|)$ we use a combination of two quadratic functions and a

var	e_H	e_J	e_S	interpretation
1	1	0	0	central value
2	2	0	0	hard scale variation
3	0.5	0	0	
4	1	0.5	0	jet scale variation
5	1	-0.5	0	
6	1	0	0.5	soft scale variation
7	1	0	-0.5	

Table 1. The scale variations in terms of the parameters in eq. (B.1).

linear function as in refs. [32, 34],

$$\mu_{\text{run}}(r, z, |\mu_H|) = \begin{cases} \mu_0 + a r^2/r_1 & r \leq r_1, \\ 2a r + b & r_1 \leq r \leq r_2, \\ |\mu_H| - a(r - r_3)^2/(r_3 - r_2) & r_2 \leq r \leq r_3, \\ |\mu_H| & r > r_3, \end{cases}$$

$$a = \frac{\mu_0 - |\mu_H|}{r_1 - r_2 - r_3}, \quad b = \frac{|\mu_H| r_1 - \mu_0(r_2 + r_3)}{r_1 - r_2 - r_3}. \quad (\text{B.2})$$

The expressions for a and b follow from demanding that μ_{run} is continuous and has a continuous derivative. The value of μ_0 determines the scales at $\tau = 0$, while $r_{1,2,3}$ determine the transition between the regions discussed above. For $\tau > r_3 \tau_{\text{max}}$, our choice for μ_{run} ensures that the resummation of logarithms of τ turns off (but π^2 resummation and threshold resummation are still present).

For the cross section integrated up to τ^c , we use the same scale choices as in eq. (B.1) with $\tau \rightarrow \tau^c$. In moment space, $\tau_{\text{max}} = 0.5$ and the equation for $\mu_{\mathcal{J}}$ is modified to

$$\mu_{\mathcal{J}}(\tau, N) = \frac{\mu_J(\tau)}{\sqrt{N} e^{\gamma_E/2}}. \quad (\text{B.3})$$

We complete our description by specifying our choice for the parameters of the profile function in eq. (B.2). Our central value corresponds to:

$$e_H = 1, \quad e_J = e_S = 0, \quad \mu_0 = 2 \text{ GeV}, \quad r_1 = \frac{4 \text{ GeV}}{Q}, \quad r_2 = 0.5, \quad r_3 = 1. \quad (\text{B.4})$$

As mentioned before, we estimate the perturbative uncertainties by a combination of separate scale variations, which are listed in table 1. In our cross section plots, we show the envelope of these variations. In the tables in app. C we give results for all the separate scale variations, allowing one to take correlations in the uncertainties into account.

C Perturbative coefficients C_j in moment space

In this appendix we give numerical results for the coefficients in eq. (4.1) at NNLL+NLO. Tables 2 and 3 contain the results for \tilde{C}_q and \tilde{C}_g , respectively. For each of the independent

scale variations in table 1 there is a separate set of \tilde{C}_j , labelled by the number in the first column. By extracting the $D_j(N, \mu = 1 \text{ GeV})$ for each of these variations, we obtain an estimate of the perturbative uncertainties for the FFs, including correlations between these uncertainties.

References

- [1] **HERMES** Collaboration, A. Airapetian *et. al.*, *Quark helicity distributions in the nucleon for up, down, and strange quarks from semi-inclusive deep-inelastic scattering*, *Phys. Rev.* **D71** (2005) 012003, [[hep-ex/0407032](#)].
- [2] **COMPASS** Collaboration, M. Alekseev *et. al.*, *Quark helicity distributions from longitudinal spin asymmetries in muon-proton and muon-deuteron scattering*, *Phys. Lett.* **B693** (2010) 227–235, [[arXiv:1007.4061](#)].
- [3] **STAR** Collaboration, G. Agakishiev *et. al.*, *Identified hadron compositions in $p+p$ and $Au+Au$ collisions at high transverse momenta at $\sqrt{s_{NN}} = 200 \text{ GeV}$* , *Phys. Rev. Lett.* **108** (2012) 072302, [[arXiv:1110.0579](#)].
- [4] **HERMES** Collaboration, A. Airapetian *et. al.*, *Leading-Order Determination of the Gluon Polarization from high- p_T Hadron Electroproduction*, *JHEP* **1008** (2010) 130, [[arXiv:1002.3921](#)].
- [5] **ATLAS** Collaboration, G. Aad *et. al.*, *Measurement of the jet fragmentation function and transverse profile in proton-proton collisions at a center-of-mass energy of 7 TeV with the ATLAS detector*, *Eur. Phys. J.* **C71** (2011) 1795, [[arXiv:1109.5816](#)].
- [6] **ATLAS** Collaboration, G. Aad *et. al.*, *Properties of jets measured from tracks in proton-proton collisions at center-of-mass energy $\sqrt{s} = 7 \text{ TeV}$ with the ATLAS detector*, *Phys. Rev.* **D84** (2011) 054001, [[arXiv:1107.3311](#)].
- [7] J. C. Collins, D. E. Soper, and G. F. Sterman, *Factorization of Hard Processes in QCD*, *Adv. Ser. Direct. High Energy Phys.* **5** (1988) 1–91, [[hep-ph/0409313](#)].
- [8] J. C. Collins and D. E. Soper, *Back-To-Back Jets in QCD*, *Nucl. Phys.* **B193** (1981) 381.
- [9] J. C. Collins and D. E. Soper, *Parton Distribution and Decay Functions*, *Nucl. Phys.* **B194** (1982) 445.
- [10] S. Albino, B. Kniehl, and G. Kramer, *Fragmentation functions for light charged hadrons with complete quark flavor separation*, *Nucl. Phys.* **B725** (2005) 181–206, [[hep-ph/0502188](#)].
- [11] S. Albino, B. Kniehl, and G. Kramer, *Fragmentation functions for K_S^0 and Λ with complete quark flavor separation*, *Nucl. Phys.* **B734** (2006) 50–61, [[hep-ph/0510173](#)].
- [12] M. Hirai, S. Kumano, T. H. Nagai, and K. Sudoh, *Determination of fragmentation functions and their uncertainties*, *Phys. Rev.* **D75** (2007) 094009, [[hep-ph/0702250](#)].
- [13] D. de Florian, R. Sassot, and M. Stratmann, *Global analysis of fragmentation functions for pions and kaons and their uncertainties*, *Phys. Rev.* **D75** (2007) 114010, [[hep-ph/0703242](#)].
- [14] D. de Florian, R. Sassot, and M. Stratmann, *Global analysis of fragmentation functions for protons and charged hadrons*, *Phys. Rev.* **D76** (2007) 074033, [[arXiv:0707.1506](#)].

- [15] S. Albino, B. Kniehl, and G. Kramer, *AKK Update: Improvements from New Theoretical Input and Experimental Data*, *Nucl. Phys.* **B803** (2008) 42–104, [[arXiv:0803.2768](#)].
- [16] Belle Collaboration, M. Leitgab, *Fragmentation functions at BELLE*, *J. Phys. Conf. Ser.* **295** (2011) 012051.
- [17] E. Farhi, *A QCD Test for Jets*, *Phys. Rev. Lett.* **39** (1977) 1587–1588.
- [18] Belle Collaboration, R. Seidl *et. al.*, *Measurement of Azimuthal Asymmetries in Inclusive Production of Hadron Pairs in e^+e^- Annihilation at $\sqrt{s} = 10.58$ GeV*, *Phys. Rev.* **D78** (2008) 032011, [[arXiv:0805.2975](#)].
- [19] M. Procura and I. W. Stewart, *Quark Fragmentation within an Identified Jet*, *Phys. Rev.* **D81** (2010) 074009, [[arXiv:0911.4980](#)].
- [20] A. Jain, M. Procura, and W. J. Waalewijn, *Parton Fragmentation within an Identified Jet at NNLL*, *JHEP* **1105** (2011) 035, [[arXiv:1101.4953](#)].
- [21] A. Jain, M. Procura, and W. J. Waalewijn, *Fully-Unintegrated Parton Distribution and Fragmentation Functions at Perturbative k_T* , *JHEP* **1204** (2012) 132, [[arXiv:1110.0839](#)].
- [22] M. Procura and W. J. Waalewijn, *Fragmentation in Jets: Cone and Threshold Effects*, [[arXiv:1111.6605](#)].
- [23] S. Catani, L. Trentadue, G. Turnock, and B. R. Webber, *Resummation of large logarithms in e^+e^- event shape distributions*, *Nucl. Phys.* **B407** (1993) 3–42.
- [24] G. P. Korchemsky and G. F. Sterman, *Power corrections to event shapes and factorization*, *Nucl. Phys.* **B555** (1999) 335–351, [[hep-ph/9902341](#)].
- [25] S. Fleming, A. H. Hoang, S. Mantry, and I. W. Stewart, *Jets from massive unstable particles: Top-mass determination*, *Phys. Rev.* **D77** (2008) 074010, [[hep-ph/0703207](#)].
- [26] M. D. Schwartz, *Resummation and NLO Matching of Event Shapes with Effective Field Theory*, *Phys. Rev.* **D77** (2008) 014026, [[arXiv:0709.2709](#)].
- [27] C. W. Bauer, S. Fleming, and M. E. Luke, *Summing Sudakov logarithms in $B \rightarrow X_s \gamma$ in effective field theory*, *Phys. Rev. D* **63** (2000) 014006, [[hep-ph/0005275](#)].
- [28] C. W. Bauer, S. Fleming, D. Pirjol, and I. W. Stewart, *An effective field theory for collinear and soft gluons: Heavy to light decays*, *Phys. Rev. D* **63** (2001) 114020, [[hep-ph/0011336](#)].
- [29] C. W. Bauer and I. W. Stewart, *Invariant operators in collinear effective theory*, *Phys. Lett. B* **516** (2001) 134–142, [[hep-ph/0107001](#)].
- [30] C. W. Bauer, D. Pirjol, and I. W. Stewart, *Soft-collinear factorization in effective field theory*, *Phys. Rev. D* **65** (2002) 054022, [[hep-ph/0109045](#)].
- [31] X. Liu, *SCET approach to top quark decay*, *Phys. Lett.* **B699** (2011) 87–92, [[arXiv:1011.3872](#)].
- [32] R. Abbate, M. Fickinger, A. H. Hoang, V. Mateu, and I. W. Stewart, *Thrust at N^3LL with Power Corrections and a Precision Global Fit for $\alpha_s(m_Z)$* , [[arXiv:1006.3080](#)].
- [33] S. Albino, B. Kniehl, G. Kramer, and W. Ochs, *Resummation of soft gluon logarithms in the DGLAP evolution of fragmentation functions*, *Phys. Rev.* **D73** (2006) 054020, [[hep-ph/0510319](#)].

- [34] C. F. Berger, C. Marcantonini, I. W. Stewart, F. J. Tackmann, and W. J. Waalewijn, *Higgs Production with a Central Jet Veto at NNLL+NNLO*, *JHEP* **1104** (2011) 092, [[arXiv:1012.4480](#)].
- [35] W. Furmanski and R. Petronzio, *Singlet Parton Densities Beyond Leading Order*, *Phys. Lett.* **B97** (1980) 437.
- [36] G. Curci, W. Furmanski, and R. Petronzio, *Evolution of Parton Densities Beyond Leading Order: The Nonsinglet Case*, *Nucl. Phys.* **B175** (1980) 27.
- [37] E. Floratos, C. Kounnas, and R. Lacaze, *Higher Order QCD Effects in Inclusive Annihilation and Deep Inelastic Scattering*, *Nucl. Phys.* **B192** (1981) 417.
- [38] R. K. Ellis, W. J. Stirling, and B. Webber, *QCD and collider physics*, *Camb. Monogr. Part. Phys. Nucl. Phys. Cosmol.* **8** (1996) 1–435.
- [39] G. Altarelli and G. Parisi, *Asymptotic Freedom in Parton Language*, *Nucl. Phys.* **B126** (1977) 298.
- [40] G. Altarelli, R. K. Ellis, G. Martinelli, and S.-Y. Pi, *Processes Involving Fragmentation Functions Beyond the Leading Order in QCD*, *Nucl. Phys.* **B160** (1979) 301.
- [41] G. Parisi, *Summing Large Perturbative Corrections in QCD*, *Phys. Lett. B* **90** (1980) 295.
- [42] G. Sterman, *Summation of Large Corrections to Short Distance Hadronic Cross-Sections*, *Nucl. Phys. B* **281** (1987) 310.
- [43] L. Magnea and G. Sterman, *Analytic continuation of the Sudakov form-factor in QCD*, *Phys. Rev. D* **42** (1990) 4222–4227.
- [44] T. O. Eynck, E. Laenen, and L. Magnea, *Exponentiation of the Drell-Yan cross section near partonic threshold in the DIS and \overline{MS} schemes*, *JHEP* **06** (2003) 057, [[hep-ph/0305179](#)].

var	τ^c	3	4	5	6	7	8
1	0.15	1.69	1.70	1.71	1.72	1.74	1.75
	0.16	1.77	1.76	1.76	1.76	1.77	1.78
	0.17	1.84	1.81	1.80	1.79	1.79	1.79
	0.18	1.89	1.86	1.83	1.82	1.81	1.80
	0.19	1.94	1.89	1.86	1.84	1.82	1.81
	0.20	1.99	1.93	1.88	1.85	1.83	1.81
2	0.15	1.73	1.73	1.73	1.74	1.76	1.77
	0.16	1.82	1.80	1.79	1.80	1.80	1.81
	0.17	1.90	1.86	1.85	1.84	1.83	1.84
	0.18	1.96	1.92	1.89	1.87	1.86	1.85
	0.19	2.02	1.96	1.92	1.89	1.88	1.87
	0.20	2.06	1.99	1.95	1.91	1.89	1.88
3	0.15	1.68	1.69	1.69	1.70	1.70	1.70
	0.16	1.74	1.73	1.72	1.71	1.70	1.69
	0.17	1.79	1.76	1.74	1.72	1.71	1.69
	0.18	1.83	1.79	1.76	1.73	1.71	1.68
	0.19	1.87	1.82	1.77	1.74	1.70	1.67
	0.20	1.90	1.84	1.78	1.74	1.70	1.67
4	0.15	1.62	1.62	1.62	1.63	1.65	1.66
	0.16	1.71	1.69	1.69	1.69	1.69	1.70
	0.17	1.78	1.75	1.74	1.73	1.73	1.74
	0.18	1.84	1.80	1.78	1.77	1.76	1.76
	0.19	1.90	1.85	1.82	1.80	1.78	1.77
	0.20	1.95	1.89	1.85	1.82	1.80	1.79
5	0.15	1.83	1.85	1.86	1.88	1.88	1.89
	0.16	1.89	1.89	1.89	1.89	1.88	1.88
	0.17	1.94	1.92	1.90	1.89	1.88	1.87
	0.18	1.98	1.94	1.92	1.90	1.88	1.87
	0.19	2.01	1.97	1.93	1.90	1.88	1.86
	0.20	2.05	1.99	1.94	1.91	1.88	1.85
6	0.15	1.84	1.85	1.85	1.86	1.87	1.88
	0.16	1.91	1.89	1.89	1.88	1.88	1.89
	0.17	1.96	1.93	1.91	1.90	1.89	1.88
	0.18	2.00	1.96	1.93	1.91	1.89	1.88
	0.19	2.04	1.98	1.94	1.92	1.89	1.88
	0.20	2.07	2.00	1.96	1.92	1.89	1.87
7	0.15	1.48	1.50	1.52	1.54	1.57	1.59
	0.16	1.59	1.60	1.60	1.62	1.63	1.65
	0.17	1.69	1.68	1.67	1.68	1.68	1.69
	0.18	1.77	1.74	1.73	1.72	1.72	1.72
	0.19	1.83	1.80	1.77	1.76	1.75	1.75
	0.20	1.89	1.84	1.81	1.79	1.77	1.76

$\tilde{C}_q :$

Table 2. $\tilde{C}_q(\tau^c, N, Q = 10.52 \text{ GeV}, \mu = 1 \text{ GeV})$ in units of nb at NNLL+NLO, with scale variations. \tilde{C}_q applies to both up and down-type quarks and was defined in eq. (4.3).

var	τ^c	3	4	5	6	7	8
1	0.15	0.257	0.167	0.112	0.079	0.057	0.042
	0.16	0.291	0.185	0.123	0.086	0.063	0.046
	0.17	0.323	0.201	0.133	0.094	0.068	0.051
	0.18	0.353	0.217	0.143	0.101	0.074	0.055
	0.19	0.382	0.232	0.153	0.107	0.079	0.060
	0.20	0.409	0.246	0.161	0.113	0.083	0.063
2	0.15	0.441	0.284	0.198	0.148	0.116	0.094
	0.16	0.486	0.307	0.212	0.157	0.123	0.099
	0.17	0.526	0.328	0.225	0.166	0.129	0.104
	0.18	0.564	0.346	0.236	0.174	0.134	0.108
	0.19	0.598	0.364	0.246	0.180	0.139	0.111
	0.20	0.630	0.379	0.255	0.186	0.143	0.115
3	0.15	0.060	0.019	-0.011	-0.030	-0.043	-0.053
	0.16	0.083	0.031	-0.004	-0.025	-0.039	-0.049
	0.17	0.106	0.042	0.004	-0.019	-0.034	-0.044
	0.18	0.128	0.054	0.011	-0.013	-0.029	-0.040
	0.19	0.149	0.065	0.019	-0.007	-0.024	-0.035
	0.20	0.169	0.076	0.026	-0.001	-0.019	-0.030
4	0.15	0.374	0.235	0.161	0.118	0.091	0.072
	0.16	0.404	0.250	0.170	0.124	0.095	0.075
	0.17	0.431	0.265	0.179	0.130	0.099	0.078
	0.18	0.457	0.278	0.186	0.135	0.103	0.081
	0.19	0.481	0.289	0.193	0.139	0.106	0.083
	0.20	0.503	0.300	0.200	0.144	0.109	0.085
5	0.15	0.086	0.045	0.012	-0.010	-0.025	-0.036
	0.16	0.131	0.073	0.032	0.007	-0.010	-0.022
	0.17	0.174	0.099	0.051	0.023	0.004	-0.008
	0.18	0.215	0.123	0.069	0.037	0.017	0.003
	0.19	0.254	0.146	0.086	0.051	0.029	0.014
	0.20	0.291	0.168	0.101	0.063	0.039	0.023
6	0.15	0.272	0.178	0.120	0.084	0.060	0.044
	0.16	0.306	0.195	0.130	0.091	0.066	0.048
	0.17	0.338	0.211	0.140	0.098	0.071	0.053
	0.18	0.368	0.227	0.149	0.104	0.076	0.057
	0.19	0.396	0.241	0.158	0.111	0.081	0.061
	0.20	0.422	0.254	0.166	0.117	0.086	0.065
7	0.15	0.236	0.153	0.103	0.073	0.053	0.039
	0.16	0.272	0.172	0.115	0.081	0.059	0.044
	0.17	0.305	0.190	0.127	0.089	0.066	0.049
	0.18	0.337	0.207	0.137	0.097	0.071	0.054
	0.19	0.368	0.223	0.147	0.104	0.077	0.058
	0.20	0.396	0.239	0.157	0.111	0.082	0.062

$\tilde{C}_g :$

Table 3. $\tilde{C}_g(\tau^c, N, Q = 10.52 \text{ GeV}, \mu = 1 \text{ GeV})$ in units of nb at NNLL+NLO, with scale variations.